MATERIALS CHARACTERIZATION FOR MICRONEEDLE-BASED MOLECULAR SENSING PLATFORM

Christopher Larson[1], Kevin Plaxco[2], and Ellis Meng[1]
[1]University of Southern California, Los Angeles, USA and
[2]University of California, Santa Barbara, USA

2024 IEEE 37th International Conference on Micro Electro Mechanical Systems (MEMS) | 979-8-3503-5792-9/24/$31.00 ©2024 IEEE | DOI: 10.1109/MEMS58180.2024.10439524

ABSTRACT

Adaptation of electrochemical aptamer-based (EAB) sensing to a microneedle format would enable clinically actionable, real-time molecular measurements via an easily applied, minimally-invasive, painless, wearable device. As a prerequisite, here we have explored what substrate materials meet the combined requirements of both microneedles and EAB sensor fabrication. Specifically, we evaluated 17 microneedle-compatible materials for adhesion with gold, the surface required for EAB functionalization. Those exhibiting satisfactory adhesion were functionalized with an aptamer sensitive to vancomycin, challenged with a range of target concentrations, and compared. Finally, we realized a microneedle sensing patch and demonstrated its function in solution and *ex vivo*.

KEYWORDS

Microneedles, aptamers, thin film gold, adhesion

INTRODUCTION

Electrochemical aptamer-based (EAB) sensors have been demonstrated for the measurement of a wide variety of molecular targets at physiologically relevant concentrations, with seconds time resolution, and with clinically-relevant specificity [1], [2]. In these sensors, DNA aptamers, selected to bind a specific target molecule, are modified with an alkanethiol at one end and a redox reporter, commonly methylene blue, at the other. The alkanethiol attaches this construct to the surface of a gold electrode, and the redox reporter enables electrochemical interrogation of its conformational state. Binding of the target molecule to the aptamer induces a conformational change, thereby changing the position and motion of the reporter relative to the electrode surface and affecting the kinetics of electron transfer between the two (Figure 1) [3]. This sensing mechanism is reversible and reagentless, enabling continuous *in situ* monitoring of rising and falling target concentrations. It is also independent of the enzymatic reactivity of the target, rendering the platform (at least theoretically) generalizable to any target. Consistent with this, EAB sensors have been demonstrated against a wide range of targets including antibiotics, chemotherapeutics, drugs of abuse, and protein biomarkers [2]–[4], with research continuing to grow the range of molecular species that can be targeted.

The wire format largely used for EAB sensors thus far requires surgical placement and has limited their *in vivo* use to acute studies [4]. Fabricating the EAB sensor on a microneedle would, in contrast, enable convenient, minimally-invasive, painless access to continuous *in vivo* measurements in target-rich interstitial fluid of the dermis [5]. While relatively mature for drug delivery applications, however, microneedle technology has only recently emerged as a format for sensing. In order to adapt EAB sensing for a microneedle format, certain material requirements must be satisfied. Specifically, the underlying microneedle material must be durable enough to puncture and safely reside in the skin, be plateable with gold for sensor fabrication, and be compatible with the chemical and electrochemical processes of EAB sensor fabrication and interrogation.

We selected a set of 17 materials based on mechanical robustness and amenability to microneedle fabrication. They were first evaluated for gold adhesion. Those exhibiting satisfactory adhesion were then functionalized as vancomycin-detecting EAB sensors and their performance was compared to gold wire control sensors. Finally, we implemented these findings in realization of a high surface area microneedle EAB sensor by modifying of an off-the-shelf drug delivery microneedle array. We demonstrated this prototype sensing patch both in solution and in porcine skin.

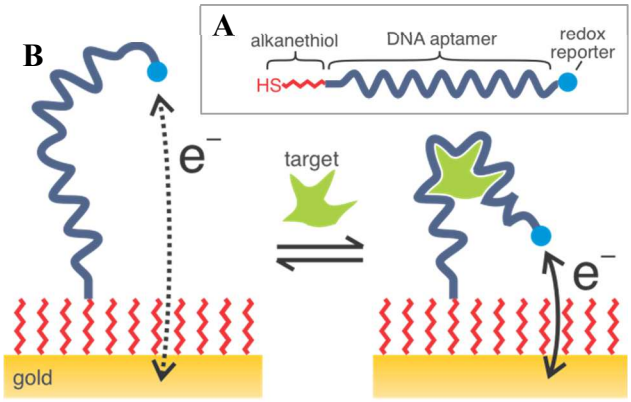

Figure 1: EAB sensing concept. A) Modified aptamer construct. B) Detection achieved via aptamer binding of target which affects kinetics of electron transfer between the redox reporter and the gold electrode.

METHODS

Materials

Vancomycin-targeting aptamer was purchased from Integrated DNA Technologies (Coralville, IA). Liquid crystal polymer plaques were provided by Celanese Corp. (Irving, TX). SLA (stereolithography) resin samples were provided by Boston Microfabrication (Maynard, MA). Parylene C dimer was purchased from SCS (Indianapolis, IN). Stainless steel, poly(methyl methacrylate) (PMMA), polyether ether ketone (PEEK), and polyetherimide (PEI) sheets and polyimide tape were purchased from McMaster. Polystyrene and all other wet and dry chemicals were purchased from VWR unless otherwise noted.

Sample Preparation

The materials tested include common MEMS and bioMEMS materials, thermoplastic polymers, and SLA

*Table 1: Materials characterized in this study for potential use in microneedle EAB sensors. *Liquid crystal polymer products from Celanese Corp. **SLA resins from Boston Microfabrication.*

MEMS/BioMEMS Materials	Glass Silicon PECVD SiO_2 316L Stainless Steel Parylene C
Thermoplastic Polymers	PMMA PEEK PEI COC Polystyrene LCP* MT1300 LCP* MT4310 LCP* MT4350 LCP* FIT30
SLA Resins	BMF** HTL BMF** HT200 BMF** BIO

resins (3D-printable photopolymers) as listed in Table 1. Glass, while not an ideal microneedle material, was included in order to evaluate the deposited gold apart from other substrate-related factors.

Planar material samples were cut into strips approximately 25 × 75 mm for adhesion tests and 4 × 40 mm for EAB sensing tests. For ease of handling, Parylene C samples were made by coating an 8 µm layer onto glass and stainless steel substrates of the same sizes. Approximately 200 nm SiO_2 was deposited onto cleaved silicon coupons by PECVD. Except for Parylene, silicon, and PECVD SiO_2, which came directly from a cleanroom environment, all samples were cleaned by ultrasonic bath in 50 °C Alconox, followed by 10-minute soaks in acetone, isopropanol, and deionized water. PMMA and polystyrene are dissolved by acetone and were thus excluded from the acetone soak. The samples were allowed to air dry, then were placed in a sealed container along with desiccant for at least 48 hours. The mass of desiccant used was approximately twice that of the samples' total. Immediately prior to metal deposition, the samples were cleaned in oxygen plasma for 300 s at 100 W and 125 mTorr with 30 sccm oxygen flow (YES-CV200RFS). 10 nm titanium and 100 nm gold were deposited by e-beam evaporation at rates of 1 Å/s and 2 Å/s respectively (Lesker PVD 75).

Wire electrodes were made by soldering 45 mm long, 200 µm diameter solid gold wires to gold-plated connector pins and insulating all but the last 6 mm with polyolefin heat-shrink tubing. To approximately match the geometric surface area of the gold wire electrode, the planar samples for EAB testing were masked with polyimide tape in which circular openings of diameter 2.2 mm were defined by laser machining.

Adhesion Testing

A cross-cut tape test was used to evaluate metal-substrate adhesion in close alignment with ASTM D3359-B [6]. Using a fresh X-Acto blade and a laser-machined acrylic guide, 11 cuts 20 mm long at a pitch of 1 mm were made through the TiAu layer, then the guide was turned 90° and 11 more cuts made. Scotch tape #600 (3M) was applied and briefly rubbed to exclude air bubbles, then rested for 60 s after which the tape was rapidly pulled back at an angle close to 180°. The resulting surface was observed under microscope whenever defects were not clear to the naked eye. Adhesion ratings from 0 (poor) to 5 (excellent) were assigned based on the percentage of metal removed by the tape.

Sensor Functionalization and Testing

Three electrodes of each substrate material were tested for compatibility with the functionalization and measurement processes of EAB sensing. Immediately prior to functionalization, all electrodes were electrochemically cleaned in 0.05 M H_2SO_4 using a Gamry Reference 600 potentiostat, Ag|AgCl reference electrode (RE), and 0.1 cm^2 platinum counter electrode (CE). 1.4 V DC was applied for 60 seconds followed by 15 cycles of cyclic voltammetry from -1.0 to +1.3 V at 0.1 V/s.

Functionalization consisted of modifying the gold surfaces with a self-assembling monolayer of aptamer as described elsewhere [7]. In brief, 100 µM solution of aptamer was prepared for gold conjugation by incubating for one hour in an excess of tris(2-carboxyethyl)phosphine (TCEP, Sigma Alrdich). The aptamer was then diluted to 500 nM in 1× phosphate-buffered saline (PBS). Electrodes were triple rinsed in deionized water and incubated in the aptamer solution for one hour. Next, the electrodes were incubated in 10 mM 6-mercapto-1-hexanol (MCH, Sigma Aldrich) in 1× PBS overnight to complete monolayer coverage of the gold. Samples and solutions were stored in the dark during all steps.

Potentiometric titration was conducted to observe the signal response of each EAB sensor. Sensors were placed in 1× PBS with 2 mM $MgCl_2$ and vancomycin concentration was increased from 0 to 1 mM (Figure 2). At each concentration, square wave voltammetry (SWV) was applied at 100 Hz from -0.1 to -0.4 V with amplitude 25 mV and step size 1 mV. The resulting voltammograms were smoothed and baseline-adjusted by a custom Python script. Successful functionalization of the electrode is indicated by an obvious peak at approximately -0.3 V which increases in amplitude with concentration.

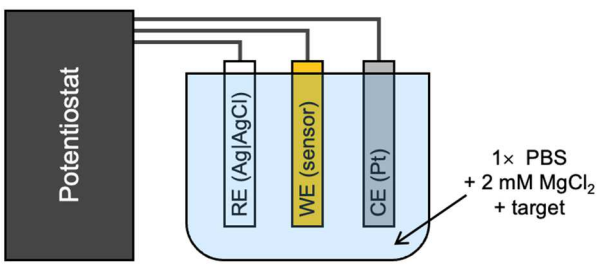

Figure 2: Three-electrode electrochemical cell for benchtop characterization of EAB sensors consisting of reference (RE), working (WE), and counter (CE) electrodes.

Microneedle EAB Sensor

AdminPatch 900 stainless steel microneedle arrays were purchased from AdminMed (Sunnyvale, CA.) An edge of each was bent to provide an unobstructed area for electrical connection, then they were conformally coated with 4 µm Parylene C. Metal was deposited as previously described. During deposition the arrays were oriented at an angle to ensure consistent coating on one side of every needle and also continuity between each needle and the connection area. An electrical lead was attached with silver epoxy, and the non-sensing margins were insulated with marine epoxy (Loctite).

Porcine ear was used as a skin model. Electrochemical measurements require conductivity among the RE, CE, and working electrode (WE), so the ear was placed in a shallow dish of 1× PBS but not fully submerged. The CE and RE were placed directly into the solution. The modified AdminPatch was inserted into the skin on the back of the ear by finger press. As this setup was not conducive to control of vancomycin concentration at the sensor site, SWV was performed only for baseline (no target) measurements.

RESULTS

As summarized in Figure 3, ten materials exhibited excellent adhesion (0% of the gold removed) in the cross-cut tape test and were carried through to further testing of their chemical and electrochemical compatibility with EAB sensor fabrication.

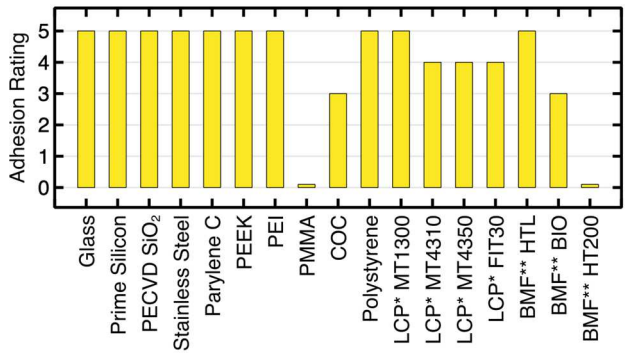

*Figure 3: Ti/Au adhesion ratings assessed using cross-cut tape test. 5 = 0% removed, 4 = <5%, 3 = 5–15%, 0 = >65%. *Liquid crystal polymer products from Celanese Corp. **SLA resins from Boston Microfabrication.*

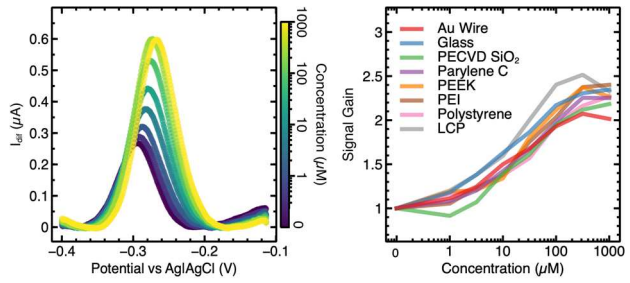

Figure 4: Left: Representative set of SWV peaks in response to vancomycin (on Parylene C substrate). Right: Comparison of average signal gain for EAB sensors made on compatible substrates (n=3).

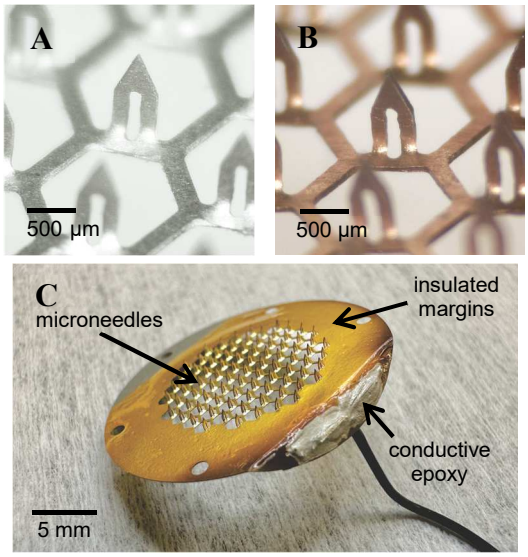

Figure 5: AdminPatch microneedle array before (A) and after (B) Parylene + Ti/Au coating. Needle height = 800 µm. C) Successfully modified and packaged prototype microneedle EAB sensor.

Three materials failed EAB compatibility testing. Metal delaminated from the HTL samples during electrochemical cleaning in H_2SO_4. Sensors on stainless steel and uninsulated silicon substrates yielded no electrochemical signal. The remaining seven materials presented strong electrochemical peaks and responded to target with signal changes comparable to those seen for gold wire controls (Figure 4).

The AdminPatch (Figure 5) was successfully modified, packaged, and demonstrated as a prototype microneedle EAB sensor. Titration with the array in solution showed strong peaks and signal gain. Peak current produced by the array was ~20× that of the gold wires, as expected due to its 20× larger surface area (Figure 6). Studies in porcine skin confirmed successful insertion (Figure 7A, B) and ability to collect baseline EAB measurements *in situ,* though peak currents were lower than those in solution by ~5× (Figure 7C).

DISCUSSION

The set of seven materials that emerged from these tests as EAB-compatible substrates allow for a wide variety of microneedle fabrication approaches, such as bulk micromachining, laser cutting, or injection molding. Failure points of the other ten materials may possibly be overcome by altering the methods used here. For example, sputtering rather than evaporating may yield better gold adhesion on some materials.

The failure of steel and uninsulated silicon to produce a signal suggests their conductivity interferes with either assembly of the aptamer monolayer (perhaps by producing a galvanic potential) or the electrochemical mechanisms of SWV. Notably, one of the EAB-compatible materials was found to be Parylene C which may be vapor-deposited as a thin conformal coating, thereby lending its compatibility to otherwise incompatible substrates. This enabled us to adapt a prefabricated stainless steel drug delivery microneedle array for use as a prototype EAB sensor.

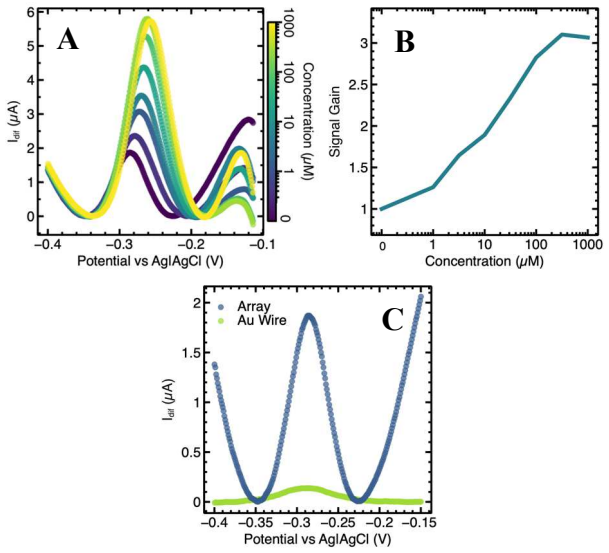

Figure 6: Demonstration of the microneedle EAB sensor in solution. A) SWV peaks increase in response to vancomycin. B) SWV peak heights plotted as signal gain. C) Peak amplitude of the array is ~20× that of a gold wire, as expected due to the ~20× higher surface area.

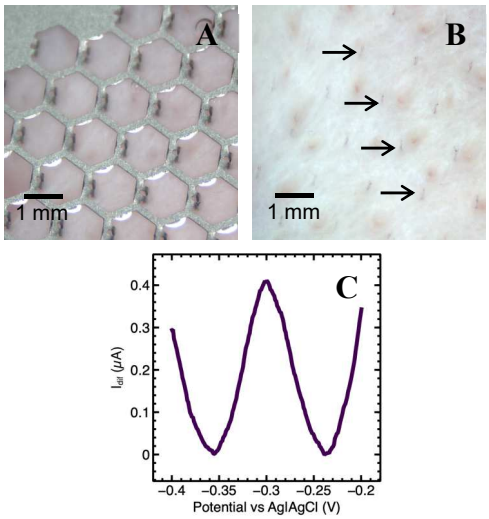

Figure 7: Demonstration of the microneedle EAB sensor in porcine ear skin. A) Top view of microneedles penetrating skin from the backside (uncoated) of the array. B) Puncture marks (arrows) visible after microneedle patch removed. C) Baseline response captured while inserted in skin, despite distant placement of the counter and reference electrodes.

Repurposing a drug-delivery microneedle patch for sensing had the advantage of high surface area (thus producing a strong signaling current), but with the disadvantage of having only a single electrode which constrained us to distant placement of the CE and RE. This arrangement was suspected as the cause of lower signal peaks in skin. To address this, future *in vivo* microneedle EAB sensors will ideally include a nearby CE and RE on the same microneedle array.

CONCLUSION

Translation of EAB sensing to a microneedle format would enable an easily-applied wearable device with broad application in physiological monitoring, able to provide actionable real-time data such as therapeutic drug, hormone, or metabolite concentrations. In the present study we laid groundwork for such an advance by confirming that evaporated thin film gold can indeed function as a surface for EAB sensor fabrication, and by establishing an initial set of materials that may serve as suitable substrates in terms of gold adhesion and chemical and electrochemical compatibility. Finally, using these findings we adapted an existing microneedle array into a working microneedle EAB sensor prototype.

ACKNOWLEDGEMENTS

This work was funded in part under Office of Naval Research grants N00014-20-1-2164 and N00014-20-1-2764. The authors thank Celanese Corp. and Boston Microfabrication for kindly providing material samples, and Kaylyn Leung, Lisa Fetter, Elsi Verrinder, and Charlotte Flatebo for providing guidance and wire electrodes.

REFERENCES

[1] Y. Xiao, A. A. Lubin, A. J. Heeger, and K. W. Plaxco, "Label-Free Electronic Detection of Thrombin in Blood Serum by Using an Aptamer-Based Sensor," *Angew. Chem. Int. Ed.*, vol. 44, no. 34, pp. 5456–5459, Aug. 2005, doi: 10.1002/anie.200500989.

[2] C. Flatebo *et al.*, "Efforts toward the continuous monitoring of molecular markers of performance," *J. Sci. Med. Sport*, vol. 26, pp. S46–S53, Jun. 2023, doi: 10.1016/j.jsams.2023.01.010.

[3] A. A. Lubin and K. W. Plaxco, "Folding-Based Electrochemical Biosensors: The Case for Responsive Nucleic Acid Architectures," *Acc. Chem. Res.*, vol. 43, no. 4, pp. 496–505, Apr. 2010, doi: 10.1021/ar900165x.

[4] N. Arroyo-Currás, J. Somerson, P. A. Vieira, K. L. Ploense, T. E. Kippin, and K. W. Plaxco, "Real-time measurement of small molecules directly in awake, ambulatory animals," *Proc. Natl. Acad. Sci.*, vol. 114, no. 4, pp. 645–650, Jan. 2017, doi: 10.1073/pnas.1613458114.

[5] P. P. Samant and M. R. Prausnitz, "Mechanisms of sampling interstitial fluid from skin using a microneedle patch," *Proc. Natl. Acad. Sci.*, vol. 115, no. 18, pp. 4583–4588, May 2018, doi: 10.1073/pnas.1716772115.

[6] D01 Committee, "Test Methods for Rating Adhesion by Tape Test," ASTM International. doi: 10.1520/D3359-22.

[7] P. Dauphin-Ducharme, K. L. Ploense, N. Arroyo-Currás, T. E. Kippin, and K. W. Plaxco, "Electrochemical Aptamer-Based Sensors: A Platform Approach to High-Frequency Molecular Monitoring In Situ in the Living Body," in *Biomedical Engineering Technologies*, vol. 2393, M. R. Ossandon, H. Baker, and A. Rasooly, Eds., in Methods in Molecular Biology, vol. 2393. , New York, NY: Springer US, 2022, pp. 479–492. doi: 10.1007/978-1-0716-1803-5_25.

CONTACT

*E. Meng; ellis.meng@usc.edu